

No excess of bright galaxies around the redshift 7.1 quasar ULAS J1120+0641

Chris Simpson^{1*}, Daniel Mortlock^{2,3}, Stephen Warren², Sebastiano Cantalupo⁴, Paul Hewett⁵, Ross McLure⁶, Richard McMahan⁵, and Bram Venemans⁷

¹*Astrophysics Research Institute, Liverpool John Moores University, Liverpool Science Park, 146 Brownlow Hill, Liverpool L3 5RF*

²*Astrophysics Group, Imperial College London, Blackett Laboratory, Prince Consort Road, London SW7 2AZ*

³*Department of Mathematics, Imperial College London, Blackett Laboratory, Prince Consort Road, London SW7 2AZ*

⁴*Department of Astronomy and Astrophysics, UCO/Lick Observatory, University of California, 1156 High Street, Santa Cruz, CA 95064, USA*

⁵*Institute of Astronomy, University of Cambridge, Madingley Road, Cambridge CB3 0HA*

⁶*Institute for Astronomy, Royal Observatory, University of Edinburgh, Blackford Hill, Edinburgh EH9 3HJ*

⁷*Max Planck Institut für Astronomie, Königstuhl 17, D-69117 Heidelberg, Germany*

Draft of 19 November 2021

ABSTRACT

We present optical and near-infrared imaging of the field of the $z = 7.0842$ quasar ULAS J112001.48+064124.3 taken with the *Hubble Space Telescope*. We use these data to search for galaxies that may be physically associated with the quasar, using the Lyman break technique, and find three such objects, although the detection of one in *Spitzer Space Telescope* imaging strongly suggests it lies at $z \sim 2$. This is consistent with the field luminosity function and indicates that there is no excess of $> L^*$ galaxies within 1 Mpc of the quasar. A detection of the quasar shortward of the Ly α line is consistent with the previously observed evolution of the intergalactic medium at $z > 5.5$.

Key words: dark ages, reionization, first stars — galaxies: active — galaxies: formation — galaxies: high redshift — quasars: individual: ULAS J1120+0641

1 INTRODUCTION

Distant quasars at $z \gtrsim 6$ are uniquely able to facilitate studies of the Universe in the first billion years after the Big Bang in two ways. First, since they are the most luminous non-transient objects, it is possible to measure the opacity of the intergalactic medium (IGM) along the line-of-sight due to absorption of photons by neutral hydrogen and probe the epoch of reionization. Second, by virtue of the fact that they already contain $\sim 10^9 M_\odot$ black holes, it is believed that quasars are located in the most overdense regions of the early Universe (e.g., Springel et al. 2005; Sijacki, Springel, & Haehnelt 2009; Costa et al. 2014; but see Fanidakis et al. 2013 for an alternative view). They should therefore act as beacons to (proto-)clusters of high-redshift galaxies and permit much more efficient observations of these galaxies.

Spectroscopy of quasars shortward of the redshifted Ly α emission line has shown a rapid increase in the optical depth from absorption at $z_{\text{abs}} > 5.5$ (Fan et al. 2006), indicating that $z \sim 6$ is the end of the epoch of reionization. When compared to the Thomson optical depth to microwave background photons, which is consistent with instantaneous reionization at $z = 11.1 \pm 1.1$ (Planck Collaboration XVI 2014), this implies that reionization was an extended and/or location-dependent process. However, due

to the large cross-sections for absorption, rest-frame far-ultraviolet spectroscopy struggles to measure the neutral hydrogen fraction, x_{HI} , if $x_{\text{HI}} \gtrsim 10^{-3}$ and so has little hope of measuring its evolution. The 21-cm hyperfine transition of H I has a much lower cross-section and therefore has diagnostic power at higher neutral fractions (Carilli, Gnedin, & Owen 2002) but it requires a bright radio source to be found at $z \gtrsim 6$ – and this has yet to happen.

The quasar ULAS J112001.48+064124.3 (hereafter ULAS J1120+0641; Mortlock et al. 2011) provided a new method of measuring the neutrality of the IGM. Discovered with a combination of infrared imaging from the UKIDSS Large Area Survey (Lawrence et al. 2007) and optical imaging from the Sloan Digital Sky Survey (SDSS; Abazajian et al. 2009), augmented with deeper imaging from the Liverpool Telescope, its redshift was originally measured as $z = 7.085 \pm 0.003$ from the broad ultraviolet emission lines, later refined to $z = 7.0842$ from a detection of the [C II] $\lambda 158 \mu\text{m}$ line by Venemans et al. (2012). While the lack of a continuum detection shortward of the Ly α emission line does not place any stringent constraints on the evolution of x_{HI} beyond the redshifts studied with SDSS quasars (Fan et al. 2006), the spectrum around the emission line displays a damping wing that implies $x_{\text{HI}} > 0.1$, and a remarkably small ionized near zone of ~ 2 Mpc in extent (Mortlock et al. 2011; Bolton et al. 2011). ULAS J1120+0641 is therefore the first quasar to be discovered within the Epoch of Reionization.

* E-mail: C.J.Simpson@ljmu.ac.uk

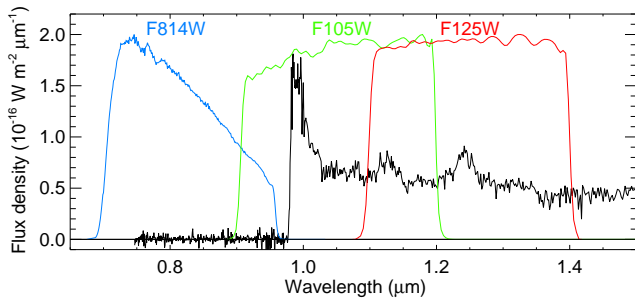


Figure 1. Spectrum of ULAS J1120+0641 (Mortlock et al. 2011), overlaid with the *HST* filters used in this work.

The environment of ULAS J1120+0641 may therefore provide an opportunity to study galaxy formation and evolution in a currently unique environment, since distant active galaxies have often been successfully used as signposts to locate overdensities in the Universe. Searches for Lyman α emitters (LAEs) and/or Lyman break galaxies (LBGs) have found excess numbers of objects around radio galaxies at $z = 4.11$ (TN J1338–1942; Venemans et al. 2002) and $z = 5.19$ (TN J0924–2201; Venemans et al. 2004; Overzier et al. 2006), and quasars at $z = 5.82$ (SDSS J0836+0054; Zheng et al. 2006) and $z = 6.28$ (SDSS J1030+0524; Stiavelli et al. 2005). In an attempt to make a more reliable statistical determination of the environments of distant quasars, Kim et al. (2009) studied *Hubble Space Telescope* (*HST*) imaging of the fields of the five most distant quasars known (at the time of their proposal), finding overdensities of high-redshift LBG candidates in two fields (including SDSS J1030+0524), and underdensities in two fields, with one field having the same sky density as seen in the Great Observatories Origins Deep Survey (GOODS). There was no clear interpretation of these results, with the underdense fields being particularly surprising since the majority of the survey volume in each field lies at a large radial distance from the quasar and so should not be affected.

Using semi-analytical prescriptions applied to the Millennium Run dark matter simulation (Springel et al. 2005), Overzier et al. (2009) find that there is sufficient scatter in the relationship between halo mass and the number of star-forming galaxies in the vicinity that even very massive haloes may not show an overdensity of galaxies. However, they do not discuss whether quasars might represent a biased, rather than a random, subset of massive haloes. The same authors note that even when there is an overdensity of galaxies, the small field of view of the *HST* Advanced Camera for Surveys may fail to reveal it. Larger fields of view are possible from the ground, but the achievable depths are brighter due to the much higher sky background. While Bañados et al. (2013) found no excess of either LBGs or LAEs around the $z = 5.72$ quasar ULAS J0203+0012 (chosen because Ly α at this redshift falls between the bright sky lines), Utsumi et al. (2010) identified an excess of LBGs around the then-most-distant known quasar, CFHQS J2329–0301 at $z = 6.43$. These objects appeared to be located in a ring at a projected proper distance of 3 Mpc, which is comparable to the size of the ionized near zones around $z \sim 6$ quasars (Carilli et al. 2010). However, the luminosities of these galaxies suggest they reside in massive subhaloes and would be unaffected by the quasar’s ionizing radiation (Kashikawa et al. 2007), so the radiation field could not explain the absence of similar galaxies at smaller quasarcentric distances.

In this paper we present *HST* imaging of the field around

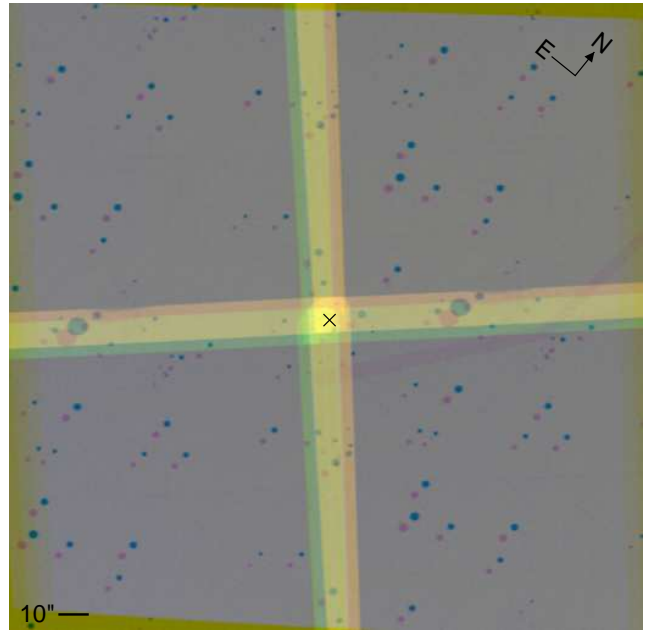


Figure 2. Exposure map of the field around ULAS J1120+0641. The blue, green, and red channels represent the exposure times in the F814W, F105W, and F125W filters, respectively. A square-root scaling has been used to better represent the relative depths, and the circular ‘blobs’ of dead pixels in the WFC3/IR detector are clearly visible. The cross indicates the location of the quasar, and a 10-arcsec scale bar is shown for scale.

ULAS J1120+0641 in three filters, designed to identify Lyman break galaxies associated with the quasar (Fig. 1). The format of this paper is as follows. In Section 2 we describe the *HST* observations and reduction, and in Section 3 we explain how we identify $z \sim 7$ galaxies. Section 4 presents a discussion of the environment of the quasar and constraints on the evolution of the Gunn–Peterson (Gunn & Peterson 1965) optical depth, while a summary of our results is provided in Section 5. We adopt a Λ CDM cosmology with $H_0 = 70 \text{ km s}^{-1} \text{ Mpc}^{-1}$ and $\Omega_m = 1 - \Omega_\Lambda = 0.3$. All magnitudes are on the AB system (Oke & Gunn 1983).

2 OBSERVATIONS AND REDUCTION

The field of ULAS J1120+0641 was observed with the Advanced Camera for Surveys (ACS) and the infrared channel of the Wide-Field Camera 3 (WFC3/IR) on board *HST*, for programme GO-13039. Due to the low ecliptic latitude of the target, all observations were performed with the LOW-SKY constraint, to reduce the sky background.

The ACS imaging was performed using the F814W filter and the Wide Field Camera (WFC) and comprised 13 orbits, spread across five visits. Four of these visits had their pointing centres sequentially offset by approximately 4 arcsec to cover the gap between the two WFC CCDs, and each visit consisted of six dithered exposures, two per orbit. A single exposure was taken in the final visit, to give a total exposure time of 28 448 s.

The WFC3/IR imaging was undertaken as a 2×2 mosaic across four visits. Within each visit, eight exposures in the F125W filter (totalling 2116 s) were taken in the first orbit, while a further eight exposures in F105W (totalling 4416 s) were split across the next two orbits. Each set of eight exposures was made in two small box dithers, separated by an offset large enough to straddle the

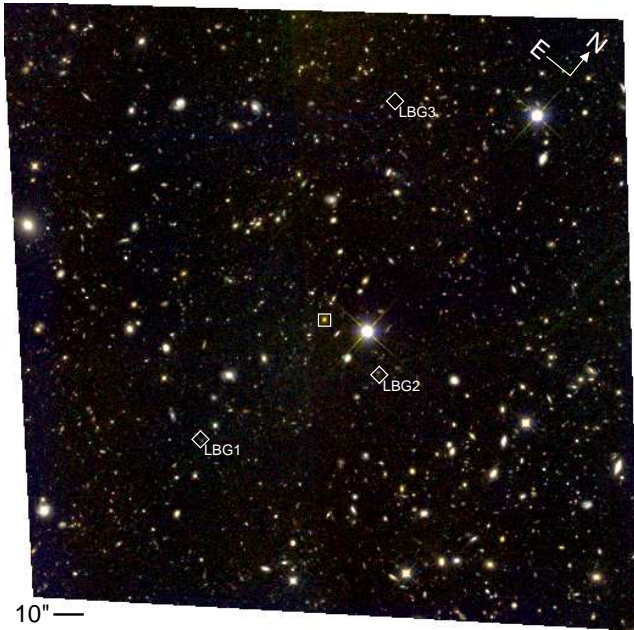


Figure 3. Combined *iJY* image of the field around ULAS J1120+0641. The quasar is indicated with a white square, while the locations of the candidate Lyman break galaxies (see Section 3.2) are marked with diamonds. The 10-arcsec scale bar represents 52 kpc (proper) at the distance of the quasar.

largest of the detector’s bad pixel ‘blobs’. Adjacent frames in the mosaic overlapped by 10 arcsec to facilitate accurate registration. This resulted in the region around the quasar itself being observed for four times longer than most of the field. Fig. 2 shows the effective exposure map produced.

The pipeline-processed images were combined using the *astrodrizzle* task in PyRAF, initially using an output pixel size equal to the input pixel size. The initial combination of the WFC3/IR data revealed the presence of astrometric offsets between the visits, due to different guide stars. These offsets were measured by combining the F105W images in each visit separately and comparing the coordinates of objects in the overlap regions. The world coordinate systems in the image headers were then updated to correct for these offsets, and new mosaics in F105W and F125W were made. We estimate the uncertainty in these corrections to be less than 10 mas by summing the offsets around the four visits in the final mosaic, which should total zero.

The combined, charge transfer efficiency-corrected ACS image revealed no such offsets, but residual structure was seen in the background, with a peak-to-peak variation of 1.5 per cent of the sky level. We investigated whether this was due to flatfielding errors by constructing a corrective flatfield from our pipelined images. All 25 ACS images were scaled to the same sky level and this stack was median filtered before the small-scale structure was removed by estimating the variation in the background with SExtractor (Bertin & Arnouts 1996). The individual images were then divided by a unity-normalized version of this frame and the new images run through *astrodrizzle*, but no improvement was seen. We also considered the possibility that the structure was due to the bias level by median-filtering the images after normalizing the sky levels by applying additive, rather than multiplicative, offsets but this had a detrimental effect on the final drizzled image. This residual structure was therefore removed from the final combined image using the SExtractor-estimated background.

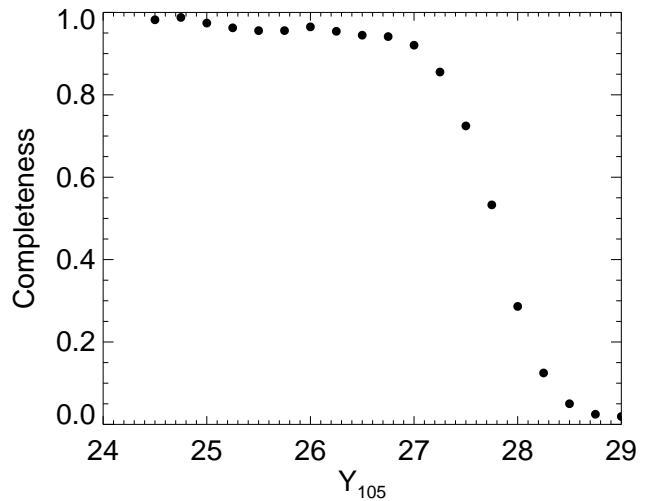


Figure 4. Completeness for $z \approx 7$ galaxies as a function of total Y_{105} magnitude, assuming galaxies have $Y_{105} - J_{125} = 0.23$. Under the assumption that $Y_{105} - J_{125} = 0.0$, all the points should be moved 0.07 mag brighter.

New versions of the two WFC3/IR mosaics were produced by drizzling them onto images with the same pixel size (0.05 arcsec) and world coordinate system as the ACS image, to improve the resolution and aid in the measurement of object colours. Object positions were then compared in each of the three images and an offset of 90 mas found between the ACS and WFC3/IR images. This was corrected by altering the headers of the ACS images and the stacked images were made a final time, with the offsets between object positions in the different filters found to be less than 20 mas.

The region of sky imaged in all three filters measures 210×225 arcsec², corresponding to a projected linear dimension of approximately 1.1 Mpc (proper) at the redshift of ULAS J1120+0641. The drizzled WFC3/IR images both have a point spread function FWHM of approximately $0''.21$, while the ACS image has a FWHM of $\sim 0''.12$. A psf-matched version of the ACS image was created by smoothing it with a Gaussian filter, and photometric measurements were made from this smoothed image. We determine the noise properties of our images by measuring the flux in 10 000 apertures placed at random locations in each image and fitting a Gaussian to the histogram of counts below $+1\sigma$. In the 0.5-arcsecond diameter apertures within which we measure colours, a signal-to-noise ratio of 3 corresponds to magnitudes of $i_{814} = 28.50$, $Y_{105} = 27.96$, and $J_{125} = 27.39$. The depth of the F814W image is limited by a combination of artifacts from the charge transfer inefficiency not fully removed by the pipeline and structure in the background on scales comparable to the extents of the brightest objects that could not be removed. A colour image made from the three individual filters is shown in Fig. 3.

3 ANALYSIS

3.1 Object detection and photometry

We follow the method of Szalay, Connolly, & Szokoly (1999) to detect objects, using a combined noise-weighted F105W+F125W image, referred to as the *R* image. SExtractor is used to find groups of contiguous pixels with values above the threshold $R = 3.35$

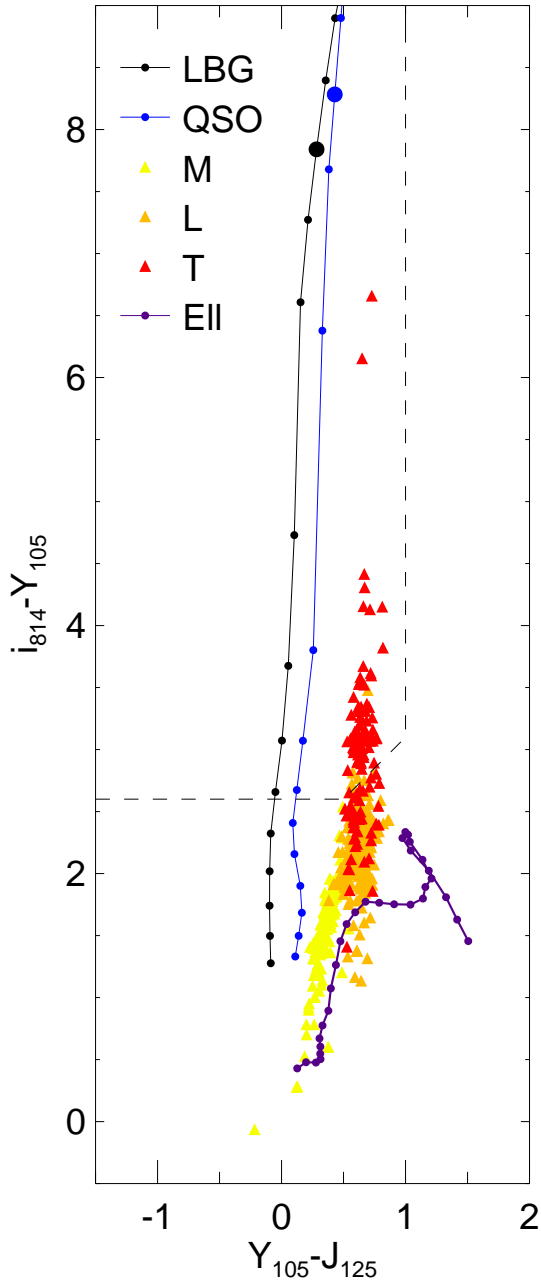


Figure 5. Colour–colour diagram used in the selection of LBGs at $z \sim 7$. The loci for $z \geq 6$ galaxies and quasars are shown by the black and blue lines, with points marked every $\Delta z = 0.1$ and large symbols at $z = 7.1$ (corresponding to the redshift of ULAS J1120+0641). The purple line shows the locus of a non-evolving elliptical galaxy over the range $0 \leq z \leq 3$, which only approaches our selection box at high redshift, $z \sim 2$, when any such galaxies will be younger and hence bluer. The locations of stars and brown dwarfs are shown by the filled triangles.

where the probabilities of misclassifying sky and object pixels are equal. By counting the number of objects detected with negative fluxes in one or both filters, we can infer the level of contamination from spurious detections for different minimum size thresholds, and adopt a value of 14 as producing a catalogue that is 97 per cent genuine, based on the number of detected sources with negative fluxes. Magnitudes are measured in circular apertures of 0.5 arcsec

diameter as well as elliptical apertures of 2.5 Kron (1980) radii, with a 0.1 mag correction applied in the manner of Oesch et al. (2010a) to account for light outside this aperture. We exclude objects detected in regions of sky where the exposure time in any filter is less than one-third of the planned exposure times listed in the previous section, and calculate an effective survey area of 11.1 arcmin².

We estimate the completeness of our catalogue by inserting artificial galaxies into the R image and finding how many we recover. The galaxies have half-light radii drawn from a normal distribution with a mean of 0.7 kpc and a standard deviation of 0.3 kpc, following Oesch et al. (2010b), with a minimum size of 0.2 kpc. Each galaxy has a Sérsic index drawn from a uniform distribution between 1.0 and 4.0 and is convolved with the point spread function measured from an isolated star. Since the F105W image is deeper, and hence more heavily weighted in the construction of the R image, the completeness is most sensitive to Y_{105} magnitude, with a secondary colour term. Assuming a colour of $Y_{105} - J_{125} = 0.23$ (see below), we obtain the points shown in Fig. 4, with 50 per cent completeness at $Y_{105} = 27.78$ (approximately $M^* + 0.4$ according to the $z \sim 7$ luminosity function of McLure et al. 2013). A colour of $Y_{105} - J_{125} = 0.0$ would cause the points to be shifted 0.07 mag brighter. The maximum completeness is 96 per cent, indicating the fraction of the image that is free from bright stars and galaxies.

3.2 Lyman break galaxies at $z \sim 7$

We model the colours of stars and galaxies through our three filters, using the SYNPHOT package available in IRAF, to determine the appropriate selection criteria for LBGs at $z \sim 7$. LBGs are modelled as 100-Myr old bursts with a constant star-formation rate, using Bruzual & Charlot (2003) models, while quasar colours are determined using the composite spectrum of Vanden Berk et al. (2001). In both cases, attenuation from the IGM was modelled in the manner of Becker, Rauch, & Sargent (2007). Colours of a non-evolving elliptical galaxy are computed from the data of Coleman, Wu, & Weedman (1980), while the colours of late-type stars and brown dwarfs are derived from the SpeX Prism Spectral Libraries.

Our selection criteria for LBGs, based on Fig. 5 are:

$$\begin{aligned} i_{814} - Y_{105} &> 2.6 \\ Y_{105} - J_{125} &< 1.0 \\ i_{814} - Y_{105} &> Y_{105} - J_{125} + 2.1 \end{aligned} \quad (1)$$

Other *HST* searches for $z \gtrsim 7$ LBGs have taken advantage of extant ultra-deep optical imaging in several bluer filters where *bona fide* LBGs will have zero flux, and which can therefore be used to reduce the number of contaminants. This enables the use of less robust colour–colour diagrams, with a smaller separation between genuine $z \sim 7$ LBGs and the key contaminants, which are $z \sim 2$ galaxies, and less depth in the ‘dropout’ filter. Since we lack such ancillary imaging, a robust sample is required from our three-colour imaging alone, and this is the reason for using F814W rather than F850LP (e.g., compare Fig. 5 to fig. 1 of Oesch et al. 2010a). Unfortunately, this precludes a standard method of analysis, as a limit of $z_{814} > 30.0$ would need to be reached to place a $Y_{105}^* = 27.4$ galaxy within our selection region. Instead, we adopt a Bayesian approach to dealing with upper limits in our F814W data. If an object has a measured flux \hat{F} , then the probability distribution for its true flux F is given by

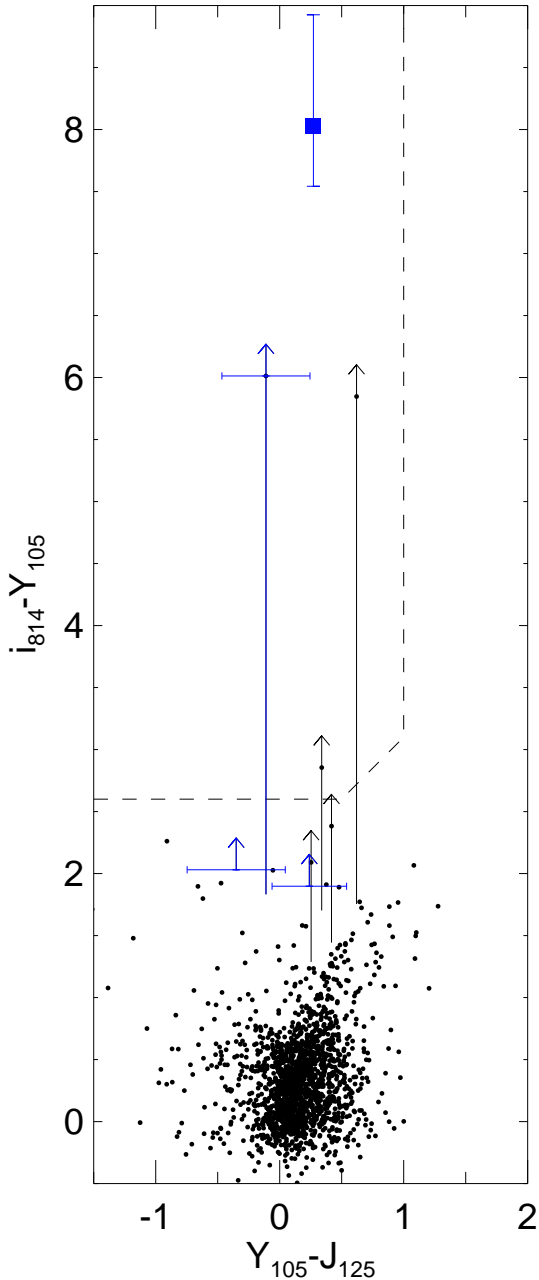


Figure 6. Colour–colour diagram for sources detected in the field of ULAS J1120+0641. Objects selected as LBGs are in blue (the quasar itself is shown by a filled square) with 1σ error bars plotted. If the 90% confidence interval on the F814W flux of an object (calculated as described in the text) includes zero, a vertical line with an upward-pointing arrow is drawn to show the extent of this confidence interval. The dashed line indicates our selection criteria for $z \sim 7$ objects, as in Fig. 5. Only objects with a signal-to-noise ratio > 5 in Y_{105} are plotted, although this criterion is not used in the selection of the LBG candidates.

$$P(F|\hat{F}) \propto P(\hat{F}|F)P(F). \quad (2)$$

If we assume that the noise is Gaussian with a standard deviation σ , which is usually true for faint objects where the observations are background-limited, then

$$P(\hat{F}|F) = \exp(-[\hat{F} - F]^2/2\sigma^2) \quad (3)$$

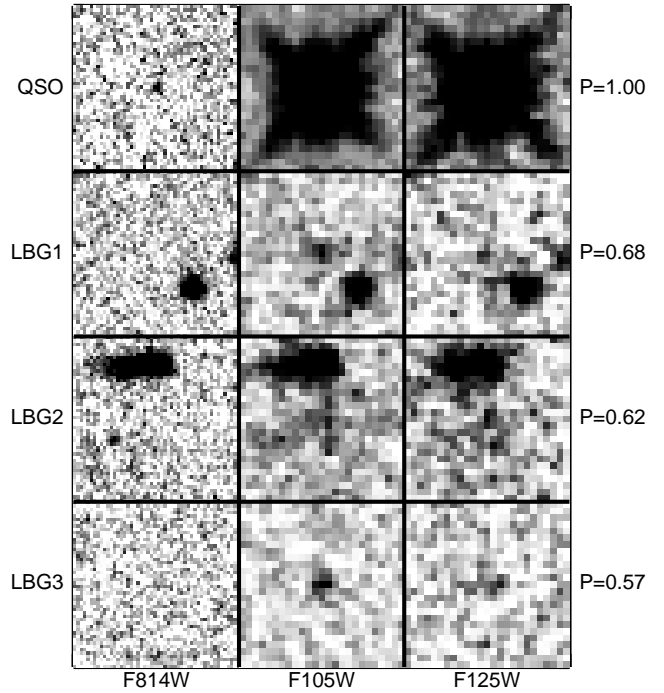


Figure 7. Images ($2.5''$ on a side) of the four objects listed in Table 1. The orientation is the same as Fig. 3, and the WFC3/IR images have been binned 2×2 . The Bayesian probabilities that these have $i_{814} - Y_{105} > 2.6$ are shown on the right-hand side of the figure.

and so, assuming a uniform prior for $F \geq 0$, we can infer the probability that the true flux of an object is fainter than some limit F_{lim} ,

$$P(F < F_{\text{lim}}|\hat{F}) = 1 - \frac{\text{erfc}([F_{\text{lim}} - \hat{F}]/\sqrt{2}\sigma)}{\text{erfc}(-\hat{F}/\sqrt{2}\sigma)} \quad (4)$$

where erfc is the complementary error function. We extend this analysis by considering the uncertainty in the Y_{105} measurement, which we assume to be Gaussian, since the limiting flux F_{lim} , in i_{814} , that we wish to consider is a function of the true Y_{105} flux (Equation 1).

In order to determine an appropriate probability above which we should consider a candidate drop-out galaxy to be plausible, we investigate how our selection criteria fare when applied to the Hubble Ultra Deep Field (HUDF). Oesch et al. (2010a) used WFC3/IR imaging in F105W and F125W plus a deep ACS F850LP image to find $z \sim 7$ galaxies, but the HUDF F814W image (Illingworth et al. 2013) is not as deep as the F850LP image and so we cannot make use of the full depth of the WFC3/IR data. Instead we set a minimum Y_{105} flux limit that is 0.4 mag deeper than the 50 per cent completeness limit in our data, as is the extra depth of the HUDF F814W data compared to ours (this is consistent with the factor of ~ 2 longer exposure time). We identify five candidate LBGs with $P \geq 0.5$, including the four brightest (in Y_{105}) sources from Oesch et al. (2010a). The remaining source, which we designate UDFi-41436012 following Oesch et al.’s naming convention, has $Y_{105} = 26.69 \pm 0.17$ and is clearly detected in F850LP but is absent in the shorter wavelength filters. McLure et al. (2013) determine a robust photometric redshift of $z = 6.45$ for this source so it fails to make their $z > 6.5$ sample, but it is a bona fide dropout. Relaxing the lower limit on P introduces sources that are demonstrably not at $z > 6$ due to their presence in the bluer images, and

Table 1. Photometry of candidate $z \sim 7$ objects selected via the Lyman break technique. The Y_{105} magnitude is a total (Kron) magnitude, while the signal-to-noise ratios and colours are measured in a 0.5-arcsecond diameter aperture. Statistical 1σ uncertainties are given, or upper limits at 90% confidence.

| ID | RA | dec | Y_{105} | $Y_{105} - J_{125}$ | $i_{814} - Y_{105}$ | SNR_i | SNR_Y | SNR_J | M_{1500} | P |
|------|-------------|-------------|------------------|---------------------|------------------------|----------------|----------------|----------------|-------------------|------|
| QSO | 11:20:01.47 | +06:41:24.0 | 20.73 ± 0.00 | 0.27 ± 0.00 | $8.03^{+0.95}_{-0.50}$ | 1.8 | 1761.7 | 1335.3 | -26.51 ± 0.00 | 1.00 |
| LBG1 | 11:20:01.93 | +06:40:27.9 | 26.34 ± 0.23 | -0.35 ± 0.40 | > 2.03 | -0.3 | 5.8 | 2.5 | -20.39 ± 0.31 | 0.68 |
| LBG2 | 11:19:59.77 | +06:41:21.2 | 25.78 ± 0.23 | 0.24 ± 0.30 | > 1.90 | -0.2 | 5.3 | 3.9 | -21.43 ± 0.21 | 0.62 |
| LBG3 | 11:20:03.30 | +06:42:34.4 | 27.23 ± 0.48 | -0.11 ± 0.36 | > 1.83 | 0.0 | 5.5 | 2.9 | -19.70 ± 0.28 | 0.57 |

Table 2. Measured flux densities in *Spitzer*/IRAC channels 1 and 2 for the three LBG candidates. Uncertainties have been determined from the root-mean-squared deviation of the counts in randomly-placed apertures and are therefore the same for all sources.

| | LBG1 | LBG2 | LBG3 | |
|-------|------|------|-------|-------------------------|
| IRAC1 | 1.45 | 5.58 | -1.06 | $\pm 0.94 \mu\text{Jy}$ |
| IRAC2 | 0.17 | 6.83 | -0.54 | $\pm 0.81 \mu\text{Jy}$ |

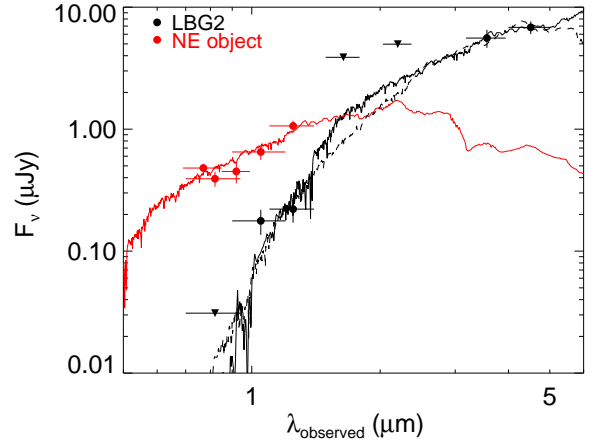
we therefore adopt $P \geq 0.50$ as the criterion for including an object in our sample of $z \sim 7$ candidates. This means that an object with zero measured flux in our F814W image will only be included in our sample if its 0.5-arcsec aperture magnitude is $Y_{105} < 27.52$, corresponding to a total magnitude of $Y_{105} \approx 27.2$.

As a final test, we add noise to the HUDF images to make their effective depths comparable to those of our quasar field and apply our detection algorithm again, now simply requiring that the flux ratio between the two filters does not exceed 5, i.e., that the signal in the detection image does not arise from only one of the WFC3/IR images. We identify only the two brightest sources from Oesch et al. (2010a), plus UDFi-41436012, over an effective area of 4.9 arcmin^2 . Applying an identical analysis to our data, we obtain the colour–colour diagram shown in Fig. 6, where four sources are detected with $P > 0.5$, one of which is the quasar itself. These are listed in Table 1 and postage stamps in each of the three filters are shown in Fig. 7. We calculate rest-frame absolute magnitudes at 1500 \AA assuming the objects lie at the same redshift as ULAS J1120+0641.

4 DISCUSSION

4.1 The environment of ULAS J1120+0641

Excluding the quasar itself, the objects we select are visually extended and therefore cannot be cool brown dwarfs. The detection of only three candidate $z \sim 7$ galaxies in our field is surprising, given that we detected the same number in the smaller (by a factor of 2.3) HUDF after making the data comparable in depth. Clearly there is no evidence for an overdensity of galaxies within 1 Mpc of the quasar, as might be expected if it is a signpost to a highly overdense region of the early Universe. Conversely, the apparent underdensity with respect to the HUDF cannot be due to the presence of the quasar since the radial extent of our survey is $\sim 250 \text{ Mpc}$, based on the predicted redshift distribution given by our selection criteria and the redshift-dependent parametrization of the field luminosity function of Bouwens et al. (2011). Using this luminosity function, and accounting for our selection function and incompleteness, we predict $5.8 z \sim 7$ galaxies in our field (we predict 2.6 in the HUDF), so there is a probability of 17 per cent that we would find three or fewer such galaxies.

**Figure 8.** Spectral energy distributions of LBG2 (black points) and the galaxy to the northeast visible in Fig. 7 (red points), with best-fitting simple stellar populations at $z = 2.49$ and $z = 0.27$, respectively, shown by solid lines. Upper limits are shown by downward-pointing triangles and include photometry from the deeper United Kingdom Infrared Telescope *H* and *K* imaging. The black dashed line shows an alternative fit to the LBG2 photometry with a much more heavily-reddened ($A_V = 1.9 \text{ mag}$) populations at $z = 1.5$.

Images of the ULAS J1120+0641 field were taken with the Infrared Array Camera (IRAC) on board the *Spitzer Space Telescope* as part of a programme to characterize the quasar’s spectral energy distribution. Inspection of these revealed a source offset by $0.4 \pm 0.2 \text{ arcsec}$ to the southwest of LBG2, i.e., away from the bright galaxy seen at the top of the postage stamps in Fig. 7, but no detections at the locations of the other LBG candidates (Table 2). We attempted to determine the nature of LBG2 and the nearby galaxy by fitting their spectral energy distributions using the photometric redshift code EAZY (Brammer, van Dokkum & Coppi 2008). We assume that all the IRAC flux arises from LBG2 and supplement the *HST* photometry of the nearby galaxy with data from Subaru/Suprime-Cam observations in the *i* and *z* filters. Using simple stellar populations from Bruzual & Charlot (2003) attenuated by Pei’s (1992) parametrization of the Small Magellanic Cloud extinction law, we obtain photometric redshifts of $z = 2.49^{+0.14}_{-1.05}$ for LBG2 and $z = 0.27^{+0.17}_{-0.18}$ for the nearby galaxy. There is a strong anti-correlation between redshift and extinction in the fit to LBG2, so lower redshift solutions require more heavily-reddened populations (see Fig. 8). All fits to LBG2 predict $Y_{105} - J_{125} \approx 1.1$, redder than observed, but consistent with the data within 3σ . These fits suggest that the IRAC photometry of LBG2 is contaminated by the nearby galaxy at a level of only a few per cent, which does not significantly affect the fit. We therefore conclude that LBG2 is most likely to be a galaxy at $z \sim 2$ and

the probability of our finding only two or fewer $z \sim 7$ galaxies in our field is 7 per cent.

Although ULAS J1120+0641 contains an extremely massive black hole that would imply a massive halo, the dynamical mass estimated by Venemans et al. (2012) from the [C II] $\lambda 158 \mu\text{m}$ line is $< 1.4 \times 10^{11} M_{\odot}$, much smaller than measured for local black holes of similar mass. This supports the idea of Willott et al. (2005) that the large scatter between the mass of the black hole and the mass of the halo in which it resides, coupled with the very steep halo mass function, makes it likely that high-redshift quasars do not sample the very massive haloes that their black hole masses would tend to suggest.

Given its depth, our data cannot rule out an excess of sub- L^* galaxies associated with the quasar. However, Stiavelli et al. (2005) found an excess of galaxy candidates around SDSS J1030+0524 despite only reaching $z_{850} = 26.5$, a full magnitude brighter than M^* at $z = 6.28$, and our data would clearly be sensitive to an abundance of galaxies that bright. It is therefore worth questioning whether the presence of the quasar could have suppressed or delayed the formation of galaxies in its immediate vicinity. This is a particularly interesting question because the strong radiation field of the quasar has an effect on the ionization state of the gas. It has been suggested that the ‘missing satellites’ problem can be explained if baryons do not cool and form stars when their dark matter haloes are below a certain mass at the time of reionization (Okamoto & Frenk 2009). Since ULAS J1120+0641 has reionized its immediate surroundings earlier than the rest of the Universe, haloes that could have formed stars elsewhere in the Universe may have been unable to do so around the quasar.

Extrapolating the spectrum of Mortlock et al. (2011) as $S_{\nu} \propto \nu^{-0.8}$, we calculate a luminosity at the Lyman limit of $L_{\nu} = 1.3 \times 10^{24} \text{ W Hz}^{-1}$, which would provide an isotropic ultraviolet intensity of $J_{\nu} \approx 3.0 \times 10^{-23} \text{ W m}^{-2} \text{ Hz}^{-1} \text{ sr}^{-1}$ at a radial distance of 550 kpc (approximately the edge of our ACS field of view), or $J_{21} \approx 30$ using the terminology of Kashikawa et al. (2007). Their calculations suggest that haloes with virial masses $M_{\text{vir}} \lesssim 10^{10} M_{\odot}$ could have their star formation significantly delayed (by $\gtrsim 100$ Myr) if exposed to a radiation field of this strength for ~ 600 Myr (the time between $z = 8.3$ and $z = 4.87$), but more massive haloes would be unaffected. Since ULAS J1120+0641 is estimated to be accreting at close to the Eddington limit (or even above it; Page et al. 2014), its luminosity in the past must have been lower. Furthermore, the small size of the quasar’s near zone suggests that the ionizing radiation has only been able to escape for a few Myr (Bolton et al. 2011), so even $M_{\text{vir}} \approx 10^{10} M_{\odot}$ haloes will have been unaffected. Since an L^* galaxy at $z \sim 7$ has a stellar mass of $\sim 10^9 M_{\odot}$ (McLure et al. 2011), it is implausible that formation of galaxies more massive than this could have been suppressed by the quasar.

We therefore consider the possibility that ULAS J1120+0641 does not reside in a massive halo. This is the scenario proposed by Fanidakis et al. (2013), who argue, based on their semi-analytic modelling, that the black holes in the most massive haloes have ended the phase where they are accreting cold gas and are highly luminous, and have already transitioned into the lower-luminosity feedback mode. This would imply that the most massive haloes at $z = 7.1$, where the galaxy overdensities lie, contain black holes as massive as that in ULAS J1120+0641 that grew to this mass more rapidly before shutting off. Given the apparent need for prolonged super-Eddington accretion to explain how this black hole reached its mass, such a model requires even more extreme accretion rates.

It is worth noting that the first $10^9 M_{\odot}$ black holes in Fanidakis et al.’s (2012) model only appear at $z < 4$ and, as a result, the model fails to reproduce the bright end of the observed quasar luminosity function at high redshift. It is therefore of questionable merit to use these models to predict the properties of the most extreme objects at $z > 7$ and, while the lack of any bright galaxy excess may be consistent with the claims of Fanidakis et al. (2013), we note that our results are also consistent with the work of Overzier et al. (2009).

4.2 The opacity of the IGM

Fig. 7 shows that the quasar is clearly detected in the F814W image, which covers the observed wavelength range $7000 \text{ \AA} < \lambda < 9600 \text{ \AA}$ ($866 \text{ \AA} < \lambda_{\text{rest}} < 1188 \text{ \AA}$) and samples wavelengths blueward of those affected by the proximity effect of the quasar. The detection of the quasar in this filter therefore gives some information on the opacity of the IGM over the redshift range $4.76 < z < 6.89$. Although the signal-to-noise ratio is only 1.8 in the 0.5-arcsecond diameter aperture through which the photometry of Table 1 is measured, a 0.25-arcsecond diameter aperture on the unsmoothed image gives a magnitude of $i_{814} = 28.59 \pm 0.20$, after applying a 30 per cent correction to account for lost flux, as determined by TinyTIM (Krist, Hook & Stoehr 2011). An aperture of this size is warranted because the position of the quasar is accurately determined from the near-infrared imaging where it is bright. We nevertheless add a 10 per cent flux uncertainty in quadrature, which accounts for a positional uncertainty of up to 50 mas.

We model the intrinsic quasar spectrum below Ly α using the quasar spectrum presented by Mortlock et al. (2011), after first scaling it to match the observed *HST* photometry. Our photometry is 14 (19) per cent fainter in the F105W (F125W) filter than derived from the spectrum using the SYNPHOT package. As the *YJ* photometry from UKIRT agrees extremely well with that derived from the spectrum we conclude that the fainter *HST* flux is due to variability between the observations. Page et al. (2014) report a factor of approximately 2 decline in the X-ray flux over a 15-month period, and a 17 per cent decrease in the far-ultraviolet flux over a period of more than 2 years (~ 100 days in the quasar rest-frame) is well within the observed variability of similarly luminous quasars (Hook et al. 1994; Welsh, Wheatley, & Neil 2011). We extend the spectrum blueward of Ly α in two ways. First, we follow Fan et al. (2006) in assuming a spectrum $S_{\nu} \propto \nu^{-0.5}$ (i.e., $\alpha_{\nu} = -0.5$), which is consistent with the mean spectrum derived from observations of the *Far Ultraviolet Spectroscopic Explorer (FUSE)* by Scott et al. (2004). Second, we extrapolate the far-ultraviolet spectrum, which is well-fit by a power-law with $\alpha_{\nu} = -0.8$, to $\lambda_{\text{rest}} = 1000 \text{ \AA}$ and then use $\alpha_{\nu} = -1.4$ at shorter wavelengths, based on *HST/Cosmic Origins Spectrograph (COS)* spectra (Shull, Stevans & Danforth 2012). Emission lines were added with equivalent widths as given in table 3 of Scott et al. (2004), and we assume that the IGM absorbs all flux at $\lambda_{\text{rest}} < 912 \text{ \AA}$.

We model the IGM absorption following Fan et al. (2006), where the effective Gunn–Peterson optical depth is given by

$$\tau_{\text{GP}}^{\text{eff}} = 0.85 \left(\frac{1+z}{5} \right)^{4.3} \quad z \leq 5.5 \quad (5)$$

$$\tau_{\text{GP}}^{\text{eff}} = 2.63 \left(\frac{1+z}{6.5} \right)^{\xi} \quad z > 5.5 \quad (6)$$

and determine the range of values of ξ that are consistent with our photometry. Fan et al. (2006) place a limit of $\xi > 10.9$ from their

spectroscopic observations. We find that values of $\xi = 10.8^{+0.6}_{-0.5}$ and $\xi = 10.6^{+0.6}_{-0.5}$ are consistent with our two models.

We also account for the opacity of the IGM in the manner of Becker et al. (2007), who model the optical depth distribution as a lognormal distribution and find a single parametrization for its evolution (without the break at $z \sim 5.5$ required by Fan et al. 2006). This model has no free parameters and predicts $i_{814} = 28.64$ and $i_{814} = 28.74$ for the $\alpha_\nu = -0.5$ and $\alpha_\nu = -0.8$ models, respectively, both of which are consistent with our measurement.

In both models, all the flux in the F814W filter is from wavelengths just above the Ly β absorption edge, where the overall opacity is lowest, and therefore we are only sensitive to the opacity at redshifts slightly larger than $z = (1 + z_{\text{qso}})\lambda_{\text{Ly}\beta}/\lambda_{\text{Ly}\alpha} - 1 = 5.82$. It is interesting to note that this is where Mortlock et al. (2011) reported the detection of flux in the quasar spectrum (an additional, less significant, transmission spike at $z = 6.68$ has subsequently been determined to not be real). However, this feature has a flux of $\sim 6 \times 10^{-21} \text{ W m}^{-2}$ (from a higher signal-to-noise ratio X-Shooter spectrum; George Becker, private communication), which is only one-half of that needed to explain the F814W flux. This implies that there must be other regions along the line of sight where the transmission is non-zero but too low to be identified in the spectrum. A tighter constraint on the evolution of the opacity requires ultra-deep imaging in a narrower filter shortward of the quasar's Ly α emission.

5 SUMMARY

We have presented new *Hubble Space Telescope* observations of the field around the $z = 7.0842$ quasar ULAS J1120+0641. We identify three candidate $z \sim 7$ galaxies from our *HST* imaging but conclude, on the basis of additional data, that only two are at this redshift, with the third being a source at $z \sim 2$. This is consistent with the number of objects expected in a blank-field survey of the same area and depth, and therefore conclude that there is no excess of $\gtrsim L^*$ galaxies within 1 Mpc of the quasar. This cannot be due to the influence of the quasar and we suggest that it is due to the small field of view of our images, as proposed by Overzier et al. (2009). The detection of the quasar in the F814W filter provides a constraint on the opacity of the IGM at $z \gtrsim 6$ and we find that the model of Becker et al. (2007) successfully reproduces the observed flux.

ACKNOWLEDGMENTS

SC acknowledges support from the NSF grant AST-1010004 and NASA *HST* grant GO-13033.06-A, RJM acknowledges ERC funding via the award of a consolidator grant, and BV has been supported by the ERC grant ‘‘Cosmic Dawn.’’ This paper is based on observations made with the NASA/ESA *Hubble Space Telescope*, obtained at the Space Telescope Science Institute, which is operated by the Association of Universities for Research in Astronomy, Inc., under NASA contract NAS 5-26555. These observations are associated with programme GO-13039, for which support was provided by NASA through a grant from the Space Telescope Science Institute. This research has benefitted from the SpeX Prism Spectral Libraries, maintained by Adam Burgasser at <http://pono.ucsd.edu/~adam/browndwarfs/spexprism>

REFERENCES

- Abazajian K. N., et al., 2009, *ApJS*, 182, 543
 Bañados E., Venemans B., Walter W., Kurk J., Overzier R., Ouchi M., 2013, *ApJ*, 773, 178
 Becker G. D., Rauch M., Sargent W. L. W., 2007, *ApJ*, 662, 72
 Bertin E., Arnouts S., 1996, *A&AS*, 117, 393
 Bolton J. S., et al., 2011, *MNRAS*, 416, L70
 Bouwens R. J., et al., 2011, *ApJ*, 737, 90
 Brammer G. B., van Dokkum P. G., Coppi P., 2008, *ApJ*, 686, 1503
 Bruzual G., Charlot S., 2003, *MNRAS*, 334, 1000
 Carilli C. L., Gnedin N. Y., Owen F., 2002, *ApJ*, 577, 22
 Carilli C. L., et al., 2010, *ApJ*, 714, 834
 Coleman G. D., Wu C.-C., Weedman D. W., 1980, *ApJS*, 43, 393
 Costa T., Sijacki D., Trenti M., Haehnelt M. G., 2014, *MNRAS*, 439, 2146
 Fan X., et al., 2006, *AJ*, 132, 117
 Fanidakis N., Macciò A. V., Baugh C. M., Lacey C. G., Frenk C. S., 2013, *MNRAS*, 436, 315
 Fanidakis N., et al., 2012, *MNRAS*, 419, 2797
 Gunn J. E., Peterson B. A., 1965, *ApJ*, 142, 1633
 Hook I. M., McMahon R. G., Boyle B. J., Irwin M. J., 1994, *MNRAS*, 268, 305
 Illingworth G. D., et al., 2013, *ApJS*, 209, 6
 Kashikawa N., Kitayama T., Doi M., Misawa T., Komiyama Y., Ota K., 2007, *ApJ*, 663, 765
 Kim S., et al., 2009, *ApJ*, 695, 809
 Krist J. E., Hook R. N., Stoehr F., 2011, *SPIE*, 8127, 16
 Kron R. G., 1980, *ApJS*, 43, 305
 Lawrence A., et al., 2007, *MNRAS*, 379, 1599
 McLure R. J., et al., 2011, *MNRAS*, 418, 2074
 McLure R. J., et al., 2013, *MNRAS*, 432, 2696
 Mortlock D. J., et al., 2011, *Nature*, 474, 616
 Oesch P. A., et al., 2010a, *ApJ*, 709, L16
 Oesch P. A., et al., 2010b, *ApJ*, 709, L21
 Okamoto T., Frenk C. S., 2009, *MNRAS*, 399, L174
 Oke J. B., Gunn J. E., 1983, *ApJ*, 266, 713
 Overzier R. A., et al., 2006, *ApJ*, 637, 58
 Overzier R. A., Guo Q., Kauffmann G., De Lucia G., Bouwens R., Lemson G., 2009, *MNRAS*, 394, 577
 Page M. J., Simpson C., Mortlock D. J., Warren S. J., Hewett P. C., Venemans B. P., McMahon R. G., 2014, *MNRAS*, 440, L91
 Pei Y. C., 1992, *ApJ*, 395, 130
 Planck Collaboration XVI, Ade P. A. R., et al., 2014, *A&A*, in press (arXiv:1303.5076)
 Scott J. E., Kriss G. A., Brotherton M., Green R. F., Hutchings J., Shull J. M., Zheng W., 2004, *ApJ*, 615, 135
 Shull J. M., Stevans M., Danforth C. W., 2012, *ApJ*, 752, 162
 Sijacki D., Springel V., Haehnelt M. G., 2009, *MNRAS*, 400, 100
 Springel V., et al., 2005, *Nature*, 435, 629
 Stiavelli M., et al., 2005, *ApJ*, 622, L1
 Szalay A. S., Connolly A. J., Szokoly G. P., 1999, *AJ*, 117, 68
 Utsumi Y., Goto T., Kashikawa N., Miyazaki S., Komiyama Y., Furusawa H., Overzier R., 2010, *ApJ*, 721, 1680
 Vanden Berk D. E., et al., 2001, *AJ*, 122, 549
 Venemans B. P., et al., 2002, *ApJ*, 569, L11
 Venemans B. P., et al., 2004, *A&A*, 424, L17
 Venemans B. P., et al., 2012, *ApJ*, 751, L25
 Welsh B. Y., Wheatley J. M., Neil J. D., 2011, *A&A*, 527, A15
 Willott C. J., Percival W. J., McLure R. J., Crampton D., Hutchings J. B., Jarvis M. J., Sawicki M., Simard L., 2005, *ApJ*, 626, 657
 Zheng W., et al., 2006, *ApJ*, 640, 574